Biomass Conversion and Biorefinery (2025) 15:10209–10224
https://doi.org/10.1007/s13399-024-05882-x

ORIGINAL ARTICLE

Theoretically supported experimental analyses on Safranin O biosorption from textile wastewater via dead biomass of *Spirogyra porticalis*

Aysun Aksu[1] · Nurşah Kütük[2] · Osman Çaylak[3] · Ergün Kasaka[4] · Serap Çetinkaya[1] · Mikhail M. Maslov[5] · Savaş Kaya[6]

Received: 16 March 2024 / Revised: 10 June 2024 / Accepted: 20 June 2024 / Published online: 11 July 2024
© The Author(s) 2024

Abstract

High-performance chemical systems designed to eliminate pollution caused by dyestuffs are still among the focuses of interest of chemists. Non-toxic biological materials especially have begun to be widely used in this field. Fourier transform infrared spectrometry, SEM (scanning electron microscopy), EDS (energy-dispersive X-ray analysis), and TGA (thermogravimetric analysis) were performed. Adsorption was performed in batch-adsorption experiments. Optimization processes involved pH, amounts of the sorbent and Safranin O, adsorption kinetics, desorption, and reusability. To highlight the mechanism of the interaction between Safranin O and *S. porticalis* and to predict the power and nature interactions, density functional theory computations were performed. Optimization processes included pH, amounts of sorbent and Safranin O, adsorption kinetics, desorption, and reusability. Experimental results were re-evaluated using Langmuir and Freundlich isotherm models and the biosorption process followed Freundlich isotherm kinetics. The biosorption mechanism was understood by pseudo-first-order (PFO), intraparticle diffusion (IPD), and Elovich models. Adsorption was determined to follow PFO kinetics: physical, endothermic, and spontaneous. The highest recovery was obtained in NaOH. Density functional theory (DFT) finding calculations were also performed to prove the high adsorption capacity for Safranin O of the material used.

Keywords Biosorption · DFT · Reactivity analysis · Safranin O · *Spirogyra porticalis* · Wastewater

1 Introduction

Water is life, but today natural water reserves are heavily polluted, especially with industrial wastewater, and their physical (color, odor, and taste) and chemical (acidity and toxicity) properties irreversibly change. The dyeing industry ranks first in terms of waste colored matter emissions [1, 2]. Colorful waters can be visually detected in rivers, lakes, and coastal seas. Waste dye contaminants can be in the form of high concentrations of natural pigments and of artificial compounds [3]. Darkish colors in water prevent the sun rays from penetrating into depths and reduce the temperature and molecular oxygen content, causing undesirable and rapid changes in flora and fauna diversity and irreparable drifts in ecological balance [4–7]. While biodiversity is decreasing, the molecular diversity in dye materials has reached tens of thousands. Blue and yellow dyes especially with their high toxicity have taken the first place due to their versatile usability. Removing these pollutants from wastewater has become a very high priority [8].

✉ Savaş Kaya
savaskaya@cumhuriyet.edu.tr

1 Science Faculty, Department of Molecular Biology and Genetics, Sivas Cumhuriyet University, 58140 Sivas, Turkey

2 Faculty of Engineering, Department of Chemical Engineering, Sivas Cumhuriyet University, Sivas, Turkey

3 Vocational School of Health Services, Department of Pharmacy, Sivas Cumhuriyet University, Sivas, Turkey

4 Yıldızeli Vocational School, Sivas Cumhuriyet University, Yıldızeli, Sivas, Turkey

5 Nanoengineering in Electronics, Spintronics and Photonics Institute, National Research Nuclear University "MEPhI", Kashirskoe Shosse, Moscow, Russia

6 Faculty of Science, Department of Chemistry, Sivas Cumhuriyet University, 58140 Sivas, Turkey

Some common purification techniques have been developed considering both the physics and chemistry of contaminating dyes. For this approach, the most favored adsorption material has been activated carbon [9–11]. The implementation costs of such and early developed approaches have typically become very high, as one can expect [12, 13]. In the following processes, viable alternative approaches have been developed by producing and testing different adsorption materials. In these approaches, the adsorption material can be single-celled organisms of plant and animal species, even in its alive form [14]. However, more commonly, the inanimate forms of these organisms have been used directly or as certain parts [15–17]. Fossil single cell remains such as dolomites have also been found among the natural adsorbent sources [18]. Crustaceans and insects have gained significant ground in the decontaminating industry as producers of natural polymers such as chitosan [19]. Plant-derived polymers have similarly become instrumental as biosorbent materials [20–22].

Particularly single-celled organisms and crustaceans, existing as a component of a particular ecosystem, where they are rightfully located, can naturally and permanently retain heavy metals and other harmful substances in their bodies at extremely high concentrations. These properties are outside the definition of biosorption and are an important reason why these organisms are sources of the biosorption material. Biosorption has already achieved significant success in laboratory-scale trials as an alternative approach for waste dye adsorption [23]. Its cost is low and its adsorption capacity is relatively higher [23]. Their inanimate forms especially played an important role in this sense [24].

Obtaining of biosorbent materials from multicellular algae requires very modest expenditure, because these organisms can spontaneously grow as large masses in natural aquatic environments, from where they are harvested directly. Multicellular algae also produce relatively larger amounts of biomass. Their cell walls constitute advantageous sources of polymer-based biosorbent substances [25–27]. In addition, various functional groups, harboring carbon, nitrogen, oxygen, and phosphorus atoms, which play the main role in the adsorption process, are abundant in the outer parts. These groups might especially create an ideal environment for the dye adsorption [28]. Here, the mechanism of adsorption might profoundly involve physical bonding forces, leading to various flocculation events [29]. Physical interactions might take place due to the high molecular weight of biopolymers and some other much smaller secondary sticky molecules, also produced by the algal cells [30].

In this study, previously collected *Spirogyra porticalis* (*S. porticalis*) biomass was used for the biosorption of Safranin O. Factors affecting biosorption, namely, pH, biosorbent dose, adsorption kinetics, and thermodynamics, as well as reusability, were investigated. Density functional theory (DFT) was used to better determine the adsorption mechanism [31].

2 Materials and method

2.1 Materials

Safranin O, ethanol (≥99%, EtOH), hydrochloric acid (≥37%, HCl), and sodium hydroxide (NaOH) were of analytical purity and obtained from Merck and Sigma-Aldrich.

2.2 Preparation of biosorbent

S. porticalis was harvested from Lake Göydün (Hafik/Sivas, Turkey) and washed under the tap water and in deionized water. Dried biomass was then pulverized [32].

2.3 Biosorbent characterization

Biosorbent surface functional groups were analyzed by Fourier transform infrared spectrometry (FTIR, ATR, Bruker, Tensor II). Its surface morphology was visualized by scanning

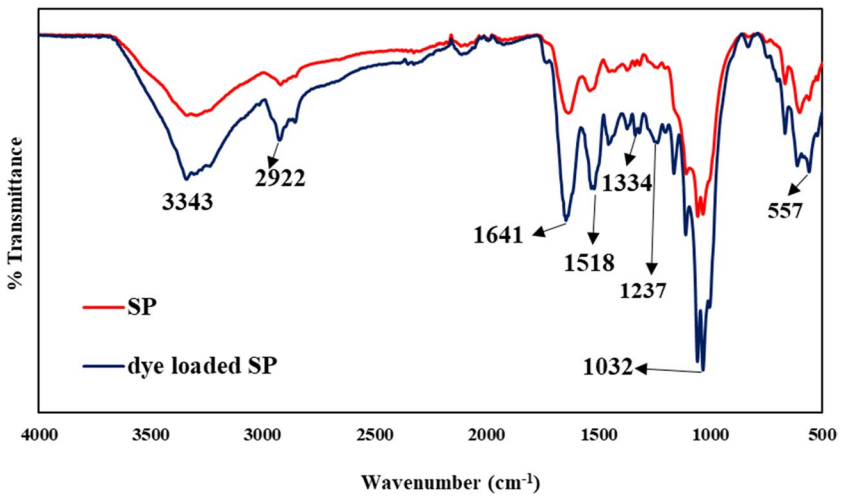


Fig. 1 FTIR spectra of *S. porticalis* before and after adsorption

electron microscopy (SEM) (TESCAN MIRA3 XMU) (CÜTAM Central Laboratory of Sivas Cumhuriyet University, Turkey). X-ray powder diffraction (XRD, Panalytical, Empyrean) and thermogravimetric analysis (TGA, Perkin Elmer, Diamond) were performed at ERÜ-TAUM (Erciyes University Technology Research and Application Centre).

2.4 Adsorption reaction

A Safranin O solution, 1000 ppm, was prepared and used in 10-mL reaction volume using the conditions below: 25 °C; adsorbent, 50 mg; and pH range 1, 3, 5, 7, 9, and 11. The reaction mixture was agitated by shaking. In kinetic experiments, dye concentrations, between 30 and 250 mg/L, and time intervals, between 10 and 1440 min, were employed. The biosorbent was precipitated by centrifugation [33], and unbound dye was estimated at 520 nm.

The biosorption efficiency (%) was computed using Eq. 1. For the biosorption capacity (q_e),

$$\text{Biosorption } \% = \left[\frac{C_o - C}{C_o}\right] \times 100 \tag{1}$$

$$q_e = \frac{(C_0 - C_e)V}{m} \tag{2}$$

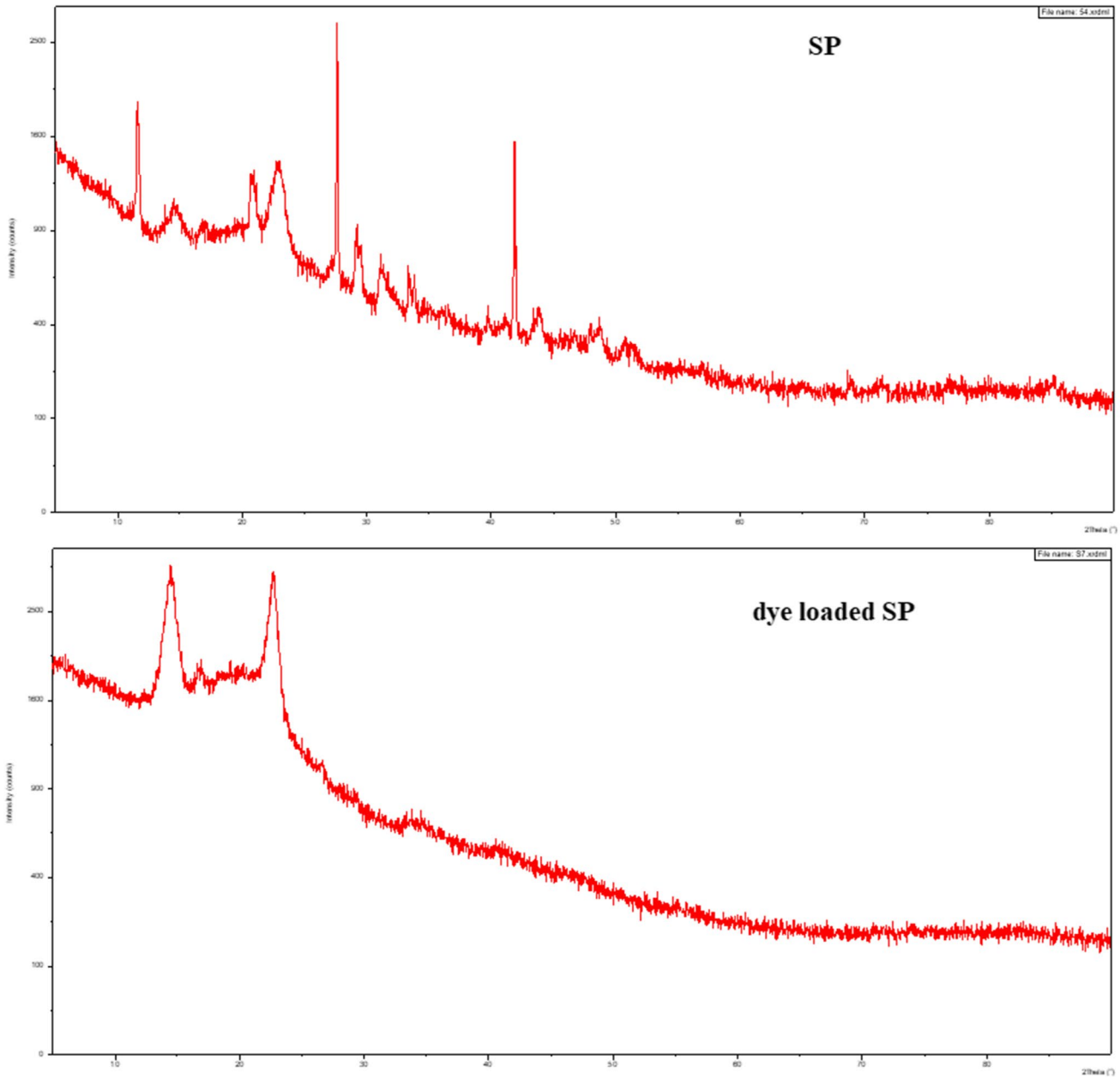


Fig. 2 XRD spectra of *S. porticalis* before and after adsorption

$$q_t = \frac{(C_0 - C_t)V}{m} \tag{3}$$

where C_0 is the initial dye concentration (mg/L), C is the dye concentration (mg/L) at time t, q_e is the biosorption capacity (mg/g) at equilibrium, q_t is the biosorption capacity (mg/g) at time t, C_e is the final dye concentration (mg/L), V is the solution volume (mL), and m is the biosorbent quantity (g).

2.5 Details of density functional theory calculations

All calculations were performed using the Perdew-Burke-Ernzerhof (GGA-PBE) exchange–correlation functional [34] and 6-31G(d) electronic basic set [35] for all elements. A graphics processor-based TeraChem software [36, 37] was used. Geometry optimization was carried out with the efficient geomeTRIC energy minimizer [38]. The dispersion corrections D3 proposed by Grimme [39] were also to take into account the weak non-covalent interactions. Conceptual density functional theory (CDFT) presents the following mathematical relations for the easy and fast calculation of the chemical reactivity descriptors such as chemical potential (μ), electronegativity (χ), hardness (η), and softness (σ).

$$\mu = -\chi = \left[\frac{\partial E}{\partial N}\right]_{v(r)} \tag{4}$$

$$\eta = \left[\frac{\partial \mu}{\partial N}\right]_{v(r)} = \left[\frac{\partial^2 E}{\partial N^2}\right]_{v(r)} \tag{5}$$

$$\sigma = 1/\eta \tag{6}$$

The given mathematical relations are based on the parabolic relation between total electronic energy (E) and total

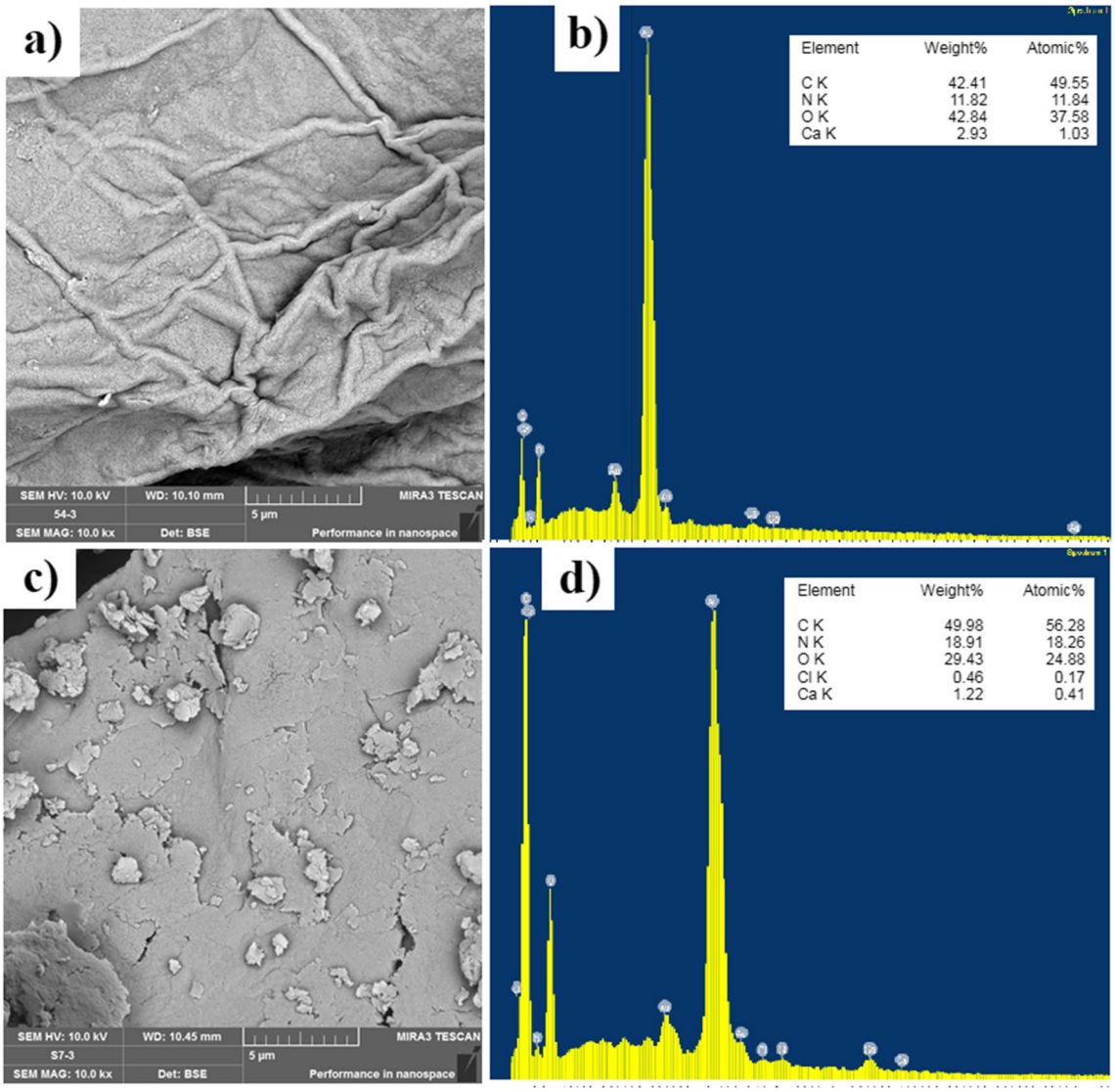


Fig. 3 SEM images. **a** *S. porticalis*. **c** Dye-loaded *S. porticalis*. EDS analysis. **b** *S. porticalis*. **d** Dye-loaded *S. porticalis*

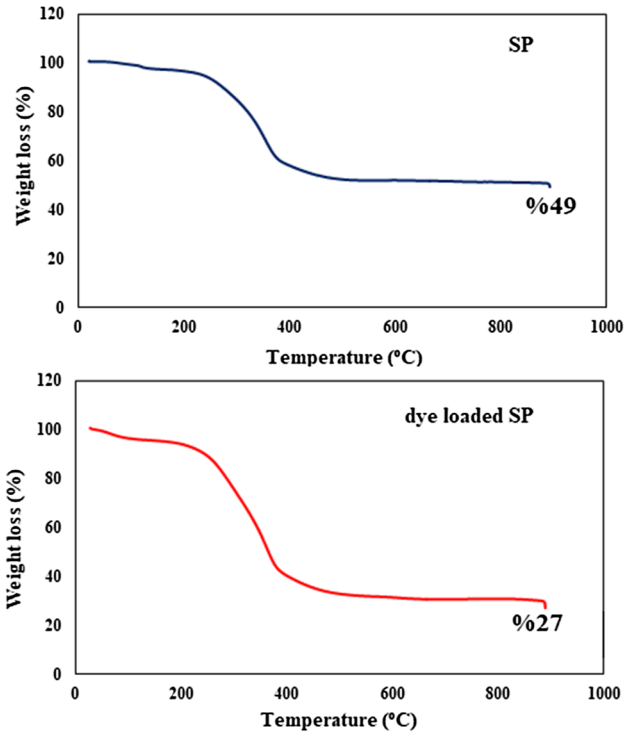


Fig. 4 TGA profiles of *S. porticalis* before and after biosorption

number of electrons (N) at a constant external potential, $\nu(r)$. If one applies the finite difference approach to the aforementioned mathematical relations, the following equations based on ground state ionization energy and electron affinity of chemical species to compute these popular reactivity descriptors [31, 40].

$$\mu = -\chi = -\left(\frac{I+A}{2}\right) \tag{7}$$

$$\eta = I - A \tag{8}$$

First and second electrophilicity indices, namely, ω_1 and ω_2, are calculated through the following equations:

$$\omega_1 = \chi^2/2\eta = (I+A)^2/8(I-A) \tag{9}$$

$$\omega_2 = I.A/I - A \tag{10}$$

In this study, we considered Koopmans theorem. This theorem can be considered as an alternative tool for the approximate calculation of ionization energy and electron affinity of molecular chemical systems based on HOMO and LUMO orbital energy from the following relations [41]:

$$I = -E_{\mathrm{HOMO}} \tag{11}$$

$$A = -E_{\mathrm{LUMO}} \tag{12}$$

3 Results and discussions

3.1 Structural analyses of the biosorbent

3.1.1 FTIR analysis

Spectra of *S. porticalis* (Fig. 1): the broad peak at 3343 cm^{-1} was attributed to the O–H stretching vibration and the N–H band [42, 43]. The vibrational band, indicating the carboxyl and phenolic group, appeared in 2922 cm^{-1} [44]. The peak at 1641 cm^{-1} represents the C = O group, the peak at 1518 cm^{-1} represents the O–H band in the quinine structure, the peak at 1334 cm^{-1} represents the N–H band, and the peak at 1237 cm^{-1} represents C-N stretching [43, 44]. The peak at 1032 cm^{-1} was attributed to the C–OH vibration band. The small peak seen at 557 cm^{-1} represents the C-N-S shear coming from the polypeptide structure [44]. Similar peaks were seen in the spectra of *S. porticalis* after biosorption. Peak of Safranin O at 3339 cm^{-1} indicated the N–H stretching vibration, and the peak at 1641 cm^{-1} represented the aromatic ring vibrational band [45]. An increase in peak intensity was evidenced due to the overlapping *S. porticalis* and Safranin O peaks.

3.1.2 XRD analysis

XRD analysis is an important characterization technique for chemical structure analysis of materials. XRD spectra of *S. porticalis* before and after biosorption are shown in Fig. 2. The crystal structure of *S. porticalis* was represented by two sharp peaks. After biosorption, these crystal peaks disappeared, and the peaks at $2\theta = 14.4°$ and 22.7° indicated that *S. porticalis* was loaded with Safranin [46].

3.1.3 SEM and EDS analyses

The surface morphology of *S. porticalis* was visualized by SEM (Fig. 3a, c) and EDS (Fig. 3b, d). SEM images produced an irregular surface topology which was consistent with those in the literature [47]. The wrinkles on *S. porticalis* before biosorption swelled and flattened after adsorption. EDS allowed an elemental analysis on the *S. porticalis* surface. Safranin O contains the elements carbon, nitrogen, and chlorine [48]. The weight and atomic percentages of these elements increased after biosorption. This observation was another proof of a successful adsorption.

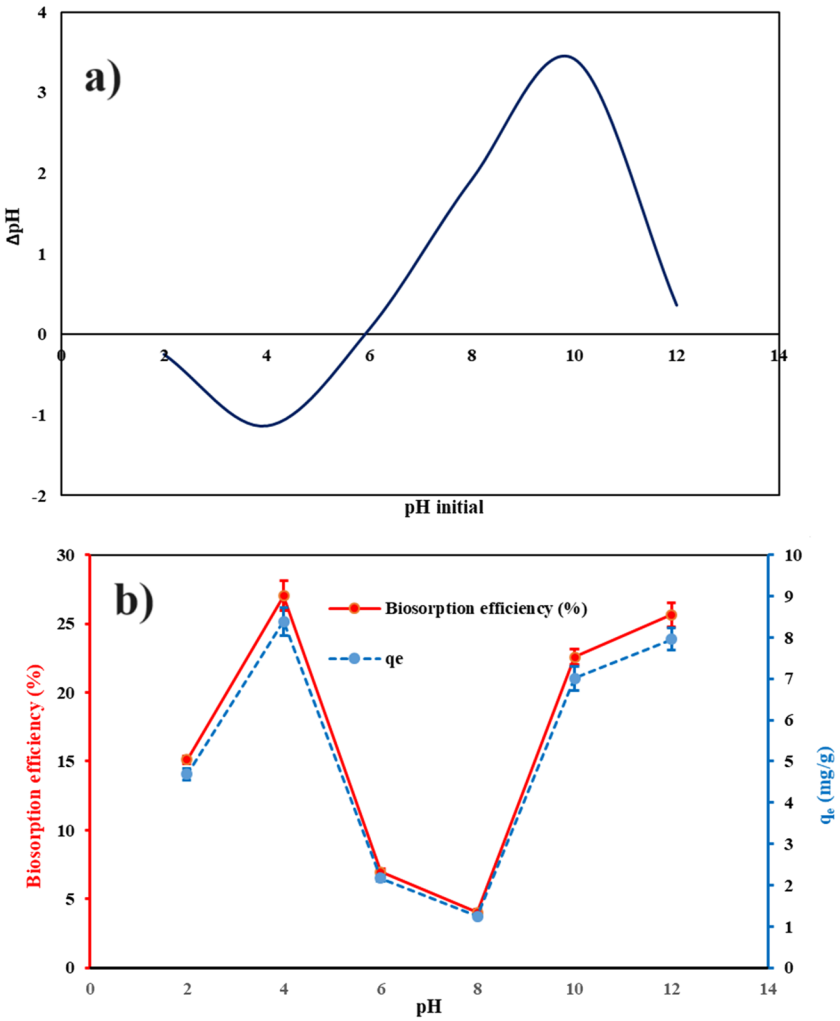


Fig. 5 **a** pH_{pzc} graphs. **b** Effect of pH on biosorption efficiency (%) and q_e ($n = 3$)

3.1.4 TGA

TGA can provide information about the temperature-dependent decomposition rate of the biosorbent, and the % weight loss versus temperature curve is given in Fig. 4. The analysis indicated that the weight loss

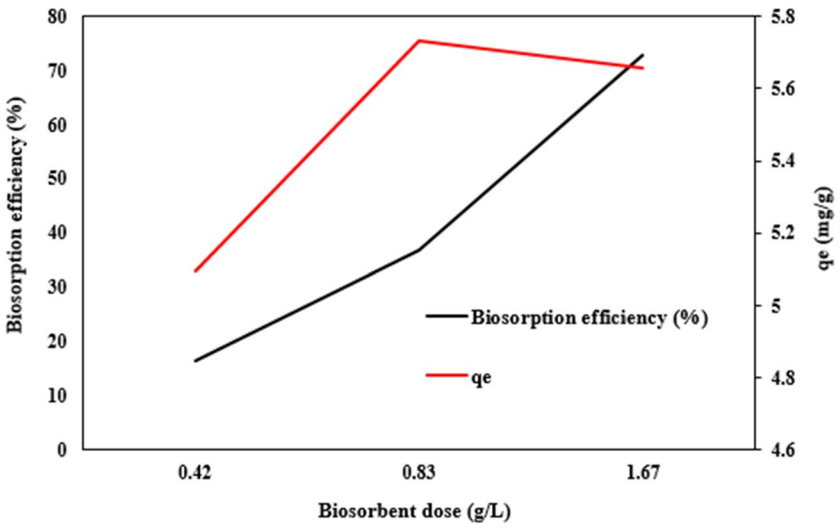


Fig. 6 Effect of biosorbent dose on biosorption efficiency (%) and q_e

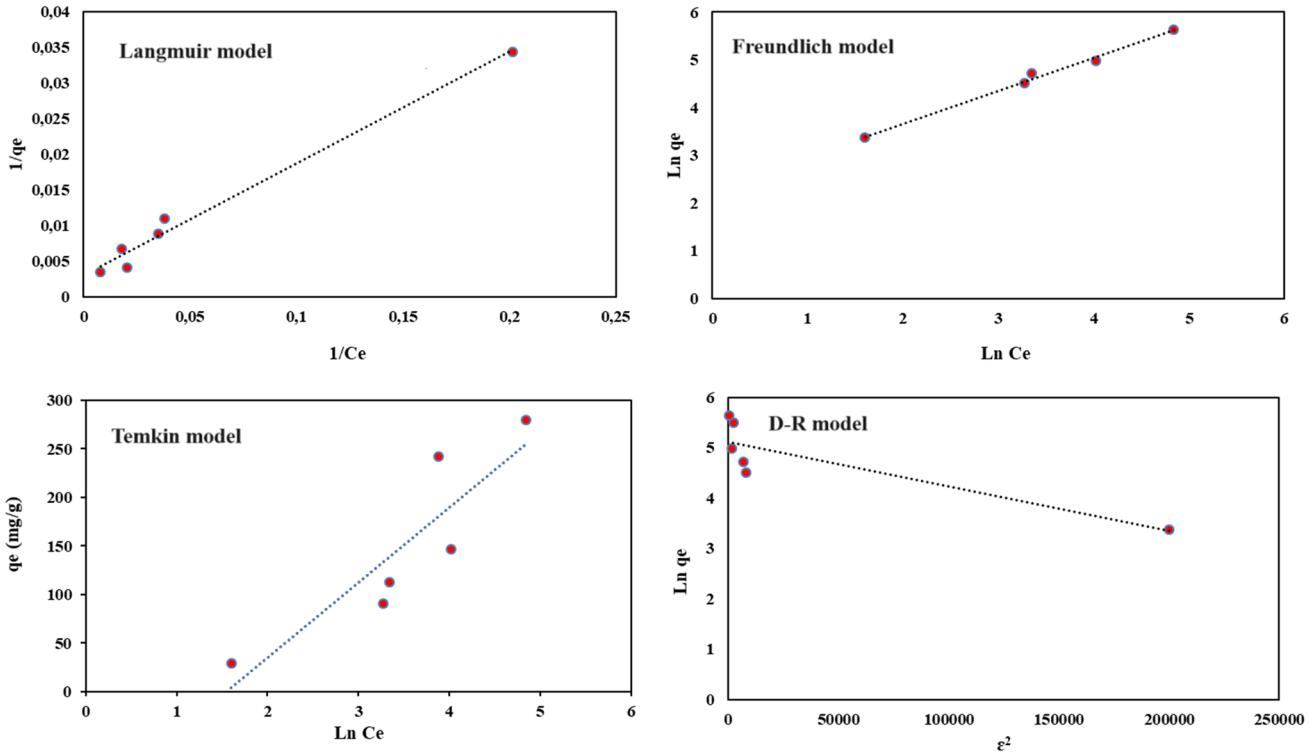


Fig. 7 Isotherm models

of *S. porticalis* increased after dye biosorption. There are two decomposition processes between 20–125 °C and 200–400 °C and represent the decomposition of water and organic part in the structure, respectively. Before adsorption, the thermal degradation was 49% and after 27%. These findings argued that *S. porticalis* biomass was not altogether temperature-resistant [47].

Table 1 Comparison of various sorbents used in Safranin O adsorption

Sorbent	q_{max}(mg/g)	References
Magnetite/Ag nanocomposite	46.3	[57]
Kaolinite	16.234	[51]
Rice straw biochar	31.06	[58]
Magnetic rice straw biochar	41.59	[58]
Immobilized *M. spicatum*-PAN/pvp hybrid beads	217.391	[59]
Magnetic *Cymopolia barbata* biomass	192.2	[60]
S. porticalis	322	This study

3.2 Biosorption procedure

3.2.1 Effect of pH on biosorption

Determination of the zero-point charge (pH_{pzc}) was carried out between pH points 2 and 12 in 0.1 M KNO_3. The differences between the initial pH and the pH after 1440 min were calculated as ΔpH and were plotted. The point that cut the *x*-axis at 5.94 and it was pH_{pzc} (Fig. 5a).

The highest biosorption efficiency was 27% at pH 4 (Fig. 5b). Fluctuation in biosorption efficiency and q_e might be due to some electrostatic interactions between the biosorbent and cationic Safranin O [48, 49], as similar findings have been reported [50]. Thus, the increase in biosorption between pH 8 and 12 could be due to the electrostatic interactions between cationic dye and negative surface of the *S. porticalis*. As the pH of the system increases, the negatively charged area on the biosorbent surface increases, so the biosorption capacity may also increase [51].

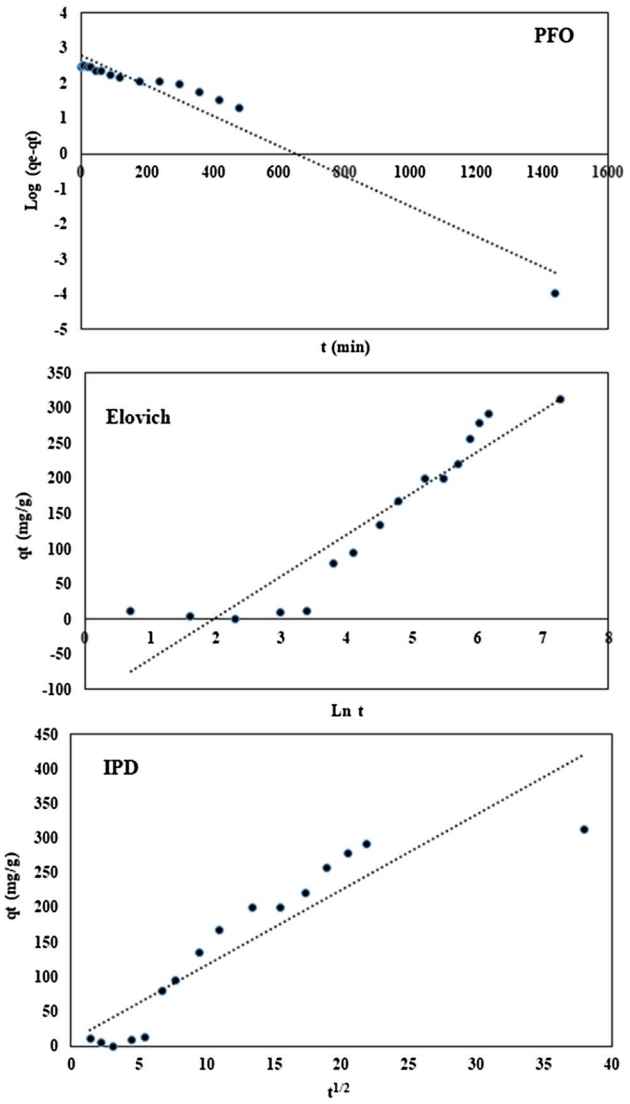


Fig. 8 Kinetic model plots for the Safranin O biosorption of SP

3.2.2 Effect of biosorbent dose on biosorption

Biosorption efficiency appeared to be proportional, up to a point, to the dose of biosorbent and then it was characterized by a slow decrease (Fig. 6). At 1.67 g/L biosorbent concentration, the highest biosorption efficiency, 73%, was achieved. However, q_e appeared to decrease slightly after 0.83 g/L biosorbent dose, at which the highest q_e value (5.73 mg/g) was reached. This phenomenon could be explained by an aggregation event, involving the biomass [52]. This result may be due to the increase in the active site responsible for sorption as the biosorbent dose increases. This result is compatible with the literature for *S. porticalis* [50].

3.2.3 Isotherm models

Safranin O biosorption of *S. porticalis* was investigated using Langmuir and Freundlich isotherm models. The Langmuir isotherm model indicates monolayer adsorption and the presence of homogeneous biosorbent structure (Eq. 13). $q_{\max}$ and K_L are the maximum biosorption capacity and Langmuir isotherm constant, respectively [53]. The Freundlich isotherm (Eq. 14) refers to multilayer biosorption and the heterogeneous surface of the biosorbent. In addition, it also indicates that the adsorption energy is not distributed uniformly between the surface molecules of the adsorbate and biosorbent [54]. K_f and n are Freundlich isotherm constants. Equation 15 formulates the Temkin isotherm and β and K_T are the constants of the Temkin isotherm. The Temkin isotherm assumes that the decrease in biosorption heat varies linearly [54]. The D-R isotherm is given in Eq. 16. ε is the Polanyi potential and is given in Eq. 17 [51]. The D-R isotherm also suggests that the biosorbent surface is formed in different sorption zones [54].

$$\frac{1}{q_e} = \frac{1}{q_{\max}} + \left(\frac{1}{K_L q_{\max}}\right)\left(\frac{1}{C_e}\right) \tag{13}$$

$$\ln q_e = \ln K_f + \left(\frac{1}{n}\right)\ln C_e \tag{14}$$

$$q_e = \beta \cdot \ln K_T + \beta \cdot \ln C_e \tag{15}$$

$$\ln q_e = \ln q_{\max} - k_D \cdot \varepsilon^2 \tag{16}$$

Table 2 Kinetic adsorption data obtained by PFO, Elovich, IPD models

Model	R^2	k_1(min^{-1})	k_i(mg·g^{-1}·min^{-2})	α(mg·g^{-1} min^{-1})	β(g·mg^{-1})
PFO	0.94	0.009			
Elovich	0.88			8.36	0.017
IPD	0.83		10.86		

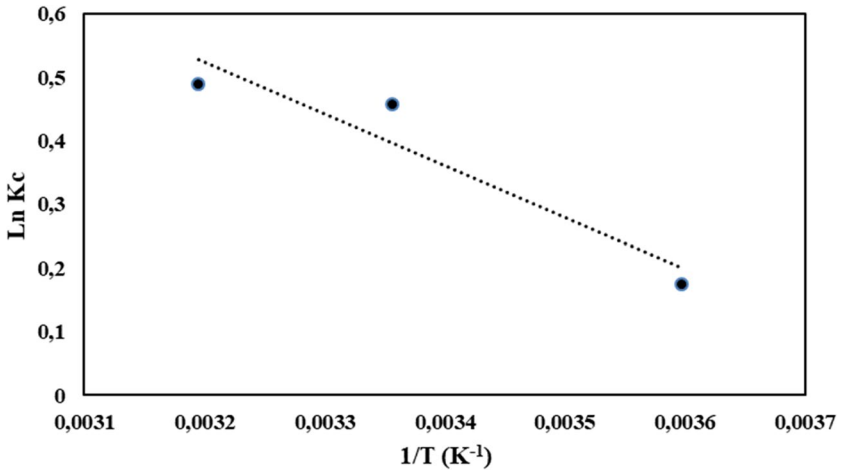


Fig. 9 Biosorption thermodynamic (C_0:100 mg/L, mass: 25 mg, contact time: 1440 min)

$$\varepsilon = RT\ln(1 + \frac{1}{C_e}) \tag{17}$$

The biosorption process was compatible with the Freundlich isotherm due to the highest R^2 value (0.99) (Fig. 7). Freundlich isotherm constant n was calculated as 1.44, and a value greater than 1 indicates the presence of physical biosorption [49]. It also means that the adsorption is favorable [55]. The K_f constant was calculated as 9.837 L/g. This finding indicated that the surface of *S. porticalis* was heterogeneous and a multi-layered biosorption has taken place [56]. It was determined that the regression value in Temkin and D-R isotherms was small at 0.8 (0.78 and 0.75, respectively). In this case, it can be said that the biosorption process does not follow these two isotherm models. According to the Langmuir isotherm ($R^2 = 0.98$), the maximum biosorption capacity (q_{max}) was calculated as 322 mg/g and the K_L value was 67.546 L/g. When Table 1 is examined, it is seen that SP has a higher q_{max} in the adsorption of Safranin O than other sorbents. In this study, SP was used as a cost-effective biosorbent without any chemical treatment.

3.2.4 Kinetic models

With the help of kinetic models, the rate of the biosorption reaction can be determined [61]. To examine the biosorption mechanism, the reaction kinetics were investigated by using the PFO (Eq. 18), intraparticle diffusion (IPD) (Eq. 19), and Elovich models (Eq. 20).

$$\log(q_e - q_t) = \log q_e - \frac{k_1}{2.303}t \tag{18}$$

$$q_t = k_{id}t^{1/2} + C \tag{19}$$

$$q_t = \frac{1}{\beta}\ln(\alpha.\beta) + \frac{1}{\beta}\ln t \tag{20}$$

It could be concluded that *S. porticalis* conformed to the PFO pattern (Fig. 8 and Table 2), where the regression value (R^2) and constant k_1 were 0.94 and 0.009 min^{-1}, respectively. These findings also indicated that a physical adsorption took place [62].

3.2.5 Biosorption thermodynamic

Temperature is an important parameter affecting the biosorption process [56]. Therefore, thermodynamic parameters such as enthalpy (ΔH), entropy (ΔS), and free energy (ΔG) were determined using Eqs. 21, 22, and 23. ln K_C versus $1/T$ data were plotted (van't Hoff graph) using Eq. 22. ΔG and ΔS data

Table 3 The van't Hoff plot of ln K_C vs. $1/T$ for the estimation of thermodynamic parameters of bioadsorption

Temp (°C)	ΔH^0 (kJ mol^{-1})	ΔS^0 (J mol^{-1} K^{-1})	ΔG^0 (kJ mol^{-1})	R^2
5	6.77	26.04	− 0.62	0.9031
25	6.77	26.04	− 1.15	
40	6.77	26.04	− 1.54	

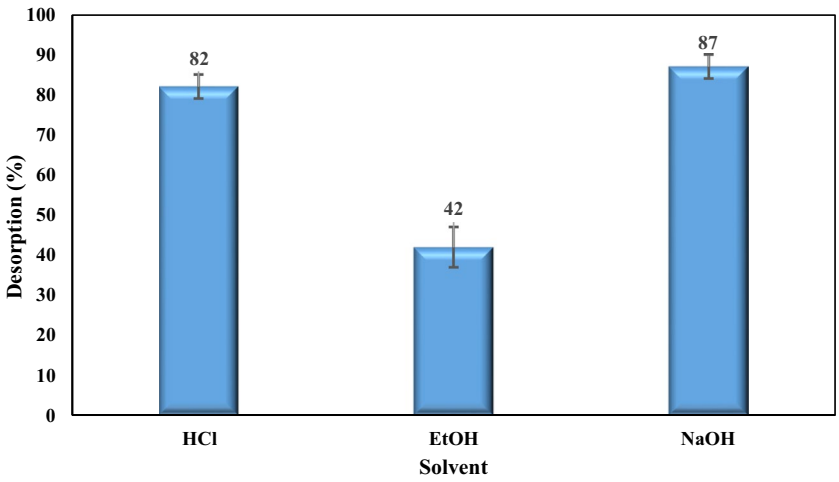


Fig. 10 Effect of type, concentration, and volume of eluent on recovery O ($n=3$) (C_0 100 mg/L, m 25 mg, temperature 25 °C, contact time 1440 min)

were calculated from slope and slip, respectively. The graph is given in Fig. 9. ΔG was calculated using Eq. 23.

$$K_C = C_a/C_e \tag{21}$$

$$\ln K_C = \frac{\Delta S}{R} - \frac{\Delta H}{R}\cdot\frac{1}{T} \tag{22}$$

$$\Delta G = \Delta H - T\Delta S \tag{23}$$

Thermodynamic data (Table 3) were calculated using Eqs. 21, 22, and 23. ΔH value was 6.77 kJ/mol and ΔS value was 26.04 J/mol·K. The positive ΔH indicated that the biosorption reaction is endothermic, and the positive ΔS indicated that the Safranin O biosorption was random at the interface between solid and liquid. Negative ΔG values indicated a spontaneous bioadsorption [63, 64].

When the mechanism of biosorption process is examined, the accumulation of dye on the heterogeneous surface of *S. porticalis* biosorbent occurs by spontaneous physical biosorption. Isotherm and kinetic models support each other.

3.2.6 Recovery

The recovery was effected in HCl, ethanol, or in NaOH by incubating 1440 min. Calculations were made using Eq. 24. The highest recovery, 87%, was achieved with 10 mL of

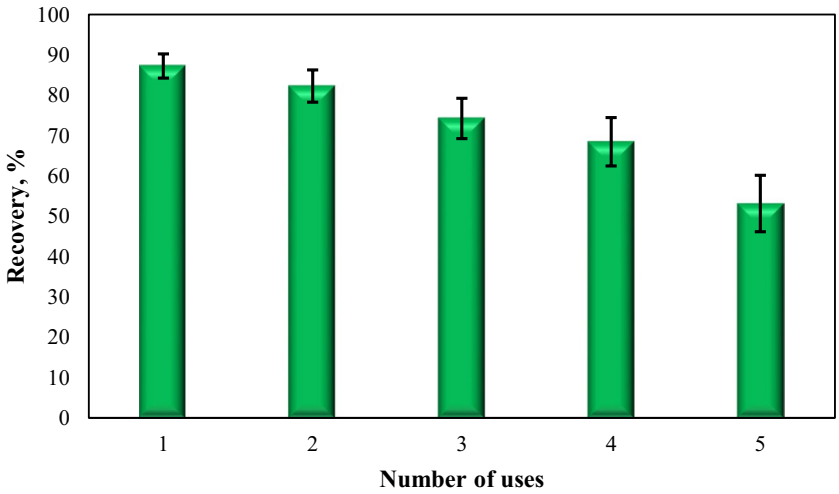


Fig. 11 Reusability of adsorbent using NaOH as eluent

Table 4 Calculated energy and electronic characteristics of *S. porticalis*, Safranin O, and their complex

Name	Dipole moment (Debye)	HOMO (eV)	LUMO (eV)	χ (eV)	η (eV)	ω_1 (eV)	Binding energy (eV)
S. porticalis	3.919	−5.222	−0.479	2.851	4.743	0.857	–
Safranin O	12.097	−3.872	−3.325	3.599	0.547	11.837	–
S. porticalis/Safranin O	9.719	−4.033	−3.388	3.711	0.645	10.673	1.152

NaOH. Also, 42% recovery in ethanol and 82% in HCl solution were achieved (Fig. 10). Figure 11 shows the reusability graph with NaOH eluent. At the end of the 5th cycle, there is a slight decrease in recovery (below 60%). This result shows that *S. porticalis* biosorbent will be efficient for several reuse cycles. Therefore, using it more than once in wastewater treatment is a good result in terms of sustainability and cost.

$$\text{Recovery}(\%)=\frac{q_{des}}{q_{ads}}\times 100 \tag{24}$$

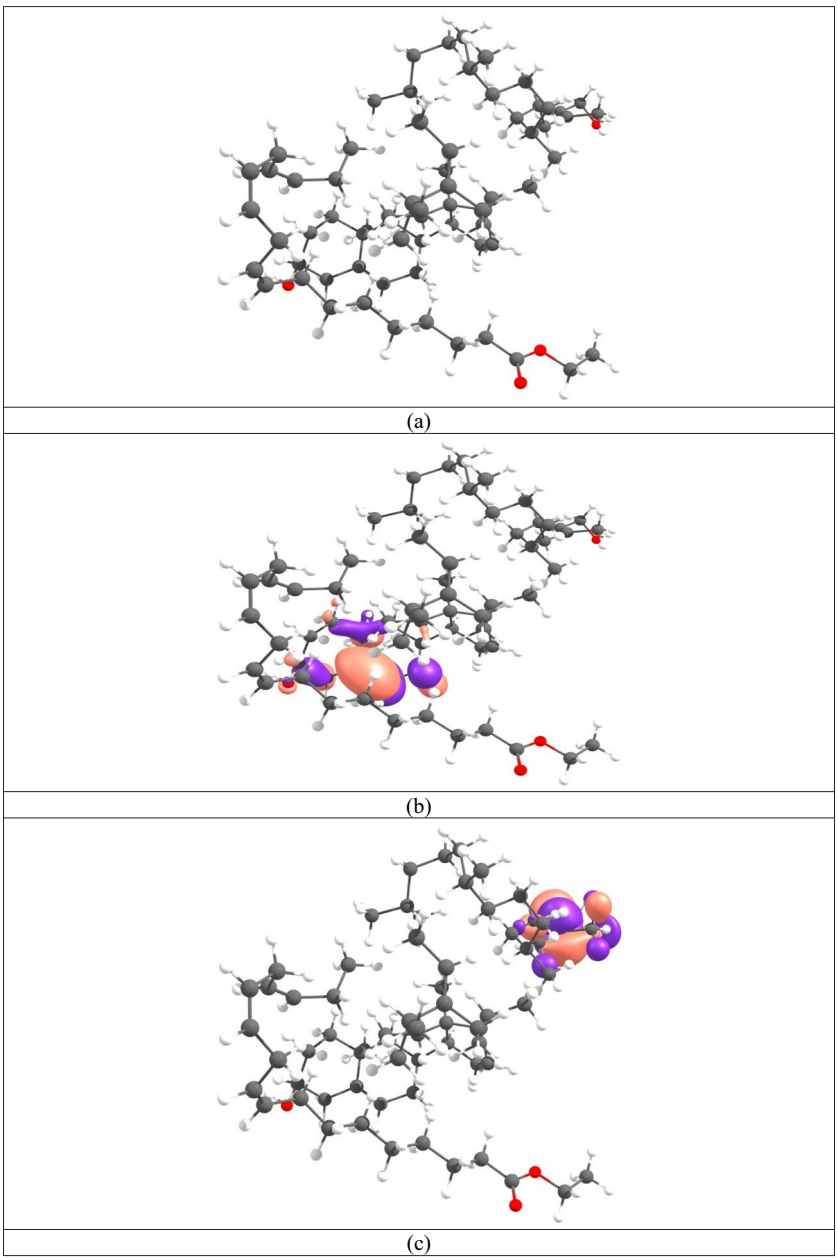


Fig. 12 Atomic model of the *S. porticalis*: **a** atomic structure, **b** HOMO, and **c** LUMO

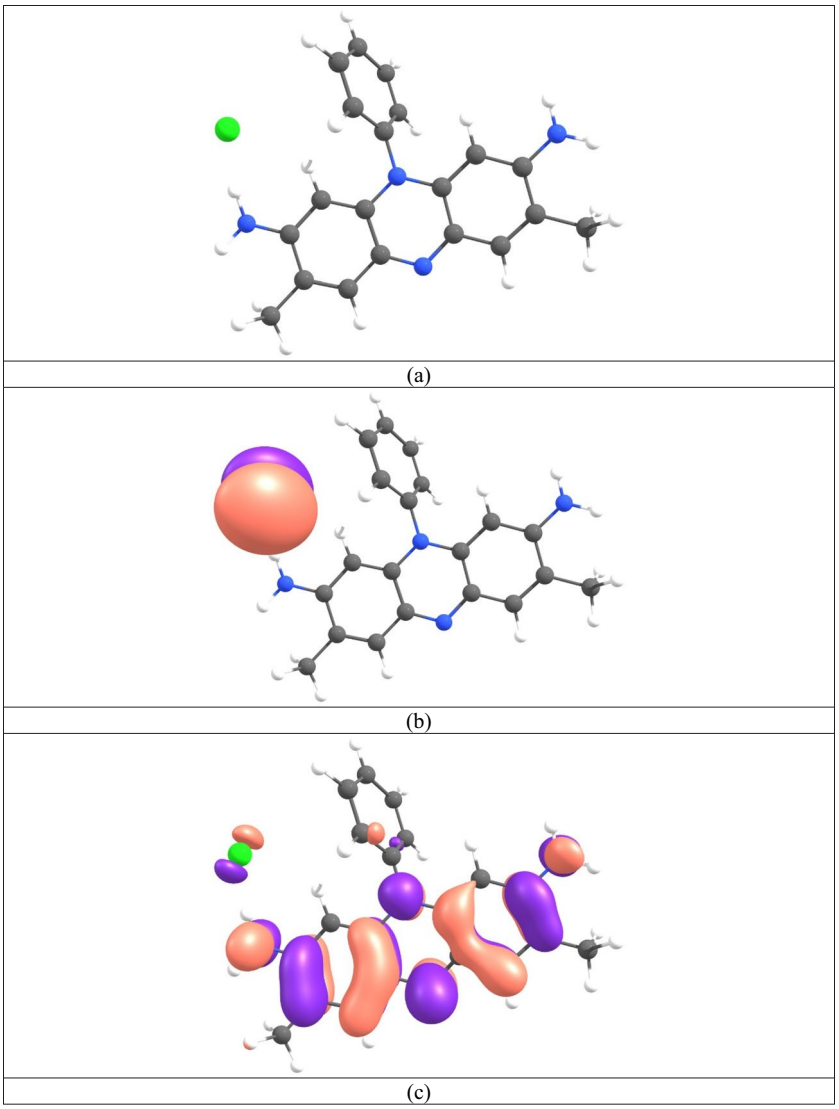


Fig. 13 Safranin O: **a** atomic structure, **b** HOMO, and **c** LUMO

3.3 Results of DFT calculations

Methanol extract of *S. porticalis* revealed the presence of thirteen different chemo types. Among these, ethyl linoleate (21.32%), stigmasta-5,24(28)-dien-3-ol, (3β) (19.55%), and 3,7,11,15-tetramethyl-2-hexadecen-1-ol (18.22%) were abundant. These three chemo types represent almost 60% of *S. porticalis.* Thus, for numerical simulation of the energy and electronic properties of the *S. porticalis*/Safranin O complex, we presented *S. porticalis* as a composition of ethyl linoleate, stigmasta-5,24(28)-dien-3-ol, (3β), and 3,7,11,15-tetramethyl-2-hexadecen-1-ol in approximately equal proportions (Fig. 11). Energy and electronic characteristics of *S. porticalis*, Safranin O, and *S. porticalis*/Safranin O complex are presented in Table 4.

The binding energy of *S. porticalis*/Safranin O complex (Fig. 13) was determined as follows:

$$E_b = E(\text{Spirogyra}) + E(\text{Safranin O}) - E(\text{Spirogyra/Safranin O}) \quad (25)$$

Calculations indicated a binding energy of 1.152 eV. The presence of the Safranin O significantly changed the electronic structure of *S. porticalis*, facilitating charge transfer and significantly reducing the gap between the frontier orbitals (Table 4). The highest occupied molecular orbital was localized on stigmasta-5,24 (28)-dien-3-ol, (3β) six-membered ring near the hydroxyl group, while the lowest unoccupied molecular orbital was localized on 3,7,11,15-tetramethyl-2-hexadecen-1-ol chain. The presence of Safranin O shifted the HOMO to the chlorine atom and part of the chain

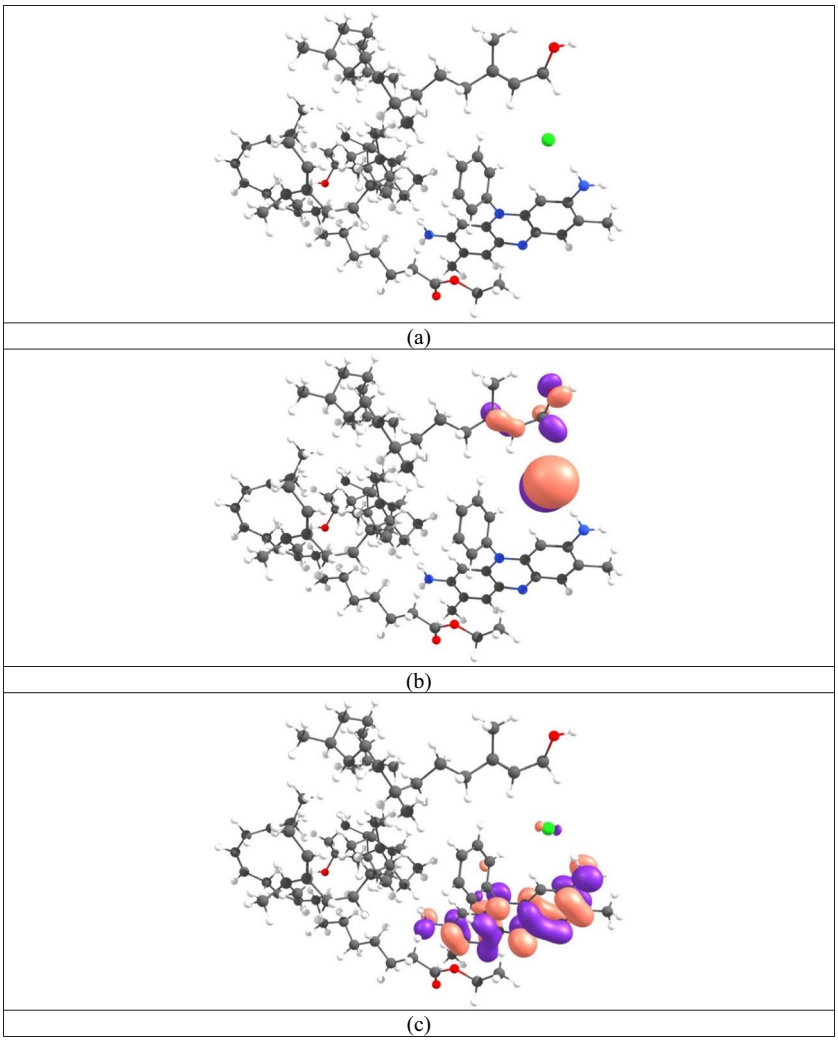


Fig. 14 Atomic model of complex consisting of *S. porticalis* and Safranin O: **a** atomic structure, **b** HOMO, and **c** LUMO

3,7,11,15-tetramethyl-2-hexadecen-1-ol chain, while LUMO was completely located on the Safranin O rings. In Fig. 11, molecular structure and HOMO and LUMO images representing *S. porticalis* are visually presented. In Fig. 12, similar images are presented for Safranin O molecule. Figure 13 includes HOMO and LUMO and molecular structure for the complex system formed with the interaction between Safranin O and *S. porticalis* (Fig. 14).

It is well known that especially chemical hardness and electrophilicity concepts provide very useful information about the chemical reactivity and stability of the chemical systems. Chemical hardness represents the resistance against the polarization of chemical systems. Within the framework of maximum hardness principle, it can be said that chemical hardness can be taken into consideration as a measure of the stability. Namely, it can be said that hard molecules exhibit higher stability than soft ones. Another electronic structure principle used in chemical reactivity analysis is minimum electrophilicity principle introduced by Chamorro, Chattaraj, and Fuentealba. This principle states that electrophilicity is minimized in stable states. With the help of the given information, it can be said that *S. porticalis* with high chemical hardness and low electrophilicity values is quite stable chemical system. On the other hand, it is clear that Safranin O with low chemical hardness and high electrophilicity is a reactive chemical system. As a result of the interaction between *S. porticalis* and Safranin O, a relatively more stable chemical system was formed compared to Safranin O.

4 Conclusion

The study showed that *S. porticalis* displayed a significant adsorption affinity to Safranin O dye in aqueous solutions. The synthesized composite was characterized by FTIR,

XRD, SEM–EDS, and TGA techniques and its structure was investigated. Parameters affecting the adsorption process were optimized. The adsorption reaction followed the Freundlich isotherm and PFO kinetic models. The adsorption was physical, and the biosorbent surface is heterogeneous and irregular. According to the Langmuir isotherm, q_{max} was calculated as 322 mg/g. The process was spontaneous and endothermic. The highest recovery occurred in NaOH. 1.152 eV was calculated for the interaction between Safranin O and the used biomass. DFT calculations supported the experimental observations. With these results, it is thought that *S. porticalis* can be used effectively in dye removal.

Author contribution Aysun Aksu: conceptualization, methodology, formal analysis, and investigation. Nurşah Kütük: conceptualization, formal analysis, investigation, and writing—review and editing. Osman Çaylak: conceptualization, formal analysis, investigation, and writing—review and editing. Ergün Kasaka: writing—original draft preparation and writing—review and editing. Serap Çetinkaya: conceptualization, methodology, formal analysis, investigation, writing—original draft preparation and writing—review and editing. Mikhail M. Maslov: conceptualization, formal analysis, and writing—review and editing. Savaş Kaya: conceptualization, formal analysis, writing—original draft preparation, and writing—review and editing.

Funding Open access funding provided by the Scientific and Technological Research Council of Türkiye (TÜBİTAK).

Data availability All data and materials supporting the results of this research are available in the article.

Declarations

Ethics approval Not applicable.

Competing interests The authors declare no competing interests.

Open Access This article is licensed under a Creative Commons Attribution 4.0 International License, which permits use, sharing, adaptation, distribution and reproduction in any medium or format, as long as you give appropriate credit to the original author(s) and the source, provide a link to the Creative Commons licence, and indicate if changes were made. The images or other third party material in this article are included in the article's Creative Commons licence, unless indicated otherwise in a credit line to the material. If material is not included in the article's Creative Commons licence and your intended use is not permitted by statutory regulation or exceeds the permitted use, you will need to obtain permission directly from the copyright holder. To view a copy of this licence, visit http://creativecommons.org/licenses/by/4.0/.

References

1. Daneshvar N, Ayazloo M, Khataee AR, Pourhassan M (2007) Biological decolorization of dye solution containing Malachite Green by microalgae *Cosmarium sp*. Biores Technol 98(6):1176–1182
2. Pakdel PM, Peighambardoust SJ (2018) A review on acrylic based hydrogels and their applications in wastewater treatment. J Environ Manage 217:123–143
3. Gupta VK, Mittal A, Gajbe V (2005) Adsorption and desorption studies of a water soluble dye, Quinoline Yellow, using waste materials. J Colloid Interface Sci 284(1):89–98
4. Pahlaviani K, Massiha A, Issazadeh K (2011) An innovative approach to biodegradation of textile azo dyes by native bacterial strains in Iran. In: International conference on biotechnology and environment management. IPCBEE 18
5. Pakdel PM, Peighambardoust SJ, ArsalaniN AH (2022) Safranin-O cationic dye removal from wastewater using carboxymethyl cellulose-grafted-poly (acrylic acid-co-itaconic acid) nanocomposite hydrogel. Environ Res 212:113201
6. Peighambardoust SJ, Boffito DC, Foroutan R, Ramavandi B (2022) Sono-photocatalytic activity of sea sediment@ 400/ZnO catalyst to remove cationic dyes from wastewater. J Mol Liq 367:120478
7. Pakdel PM, Peighambardoust SJ (2018) Review on recent progress in chitosan-based hydrogels for wastewater treatment application. Carbohyd Polym 201:264–279
8. Brahmbhatt NH, Jasrai RT (2015) Biodecolorization of reactive dyes by spirogyra sp. & oscillatoria sp. Int J Eng Res Gen Sci 3:854–859
9. Namasivayam C, Kavitha D (2002) Removal of Congo Red from water by adsorption onto activated carbon prepared from coir pith, an agricultural solid waste. Dyes Pigm 54(1):47–58
10. Banat F, Al-Asheh S, Al-Makhadmeh L (2003) Evaluation of the use of raw and activated date pits as potential adsorbents for dye containing waters. Process Biochem 39(2):193–202
11. Panahi FH, Peighambardoust SJ, Davaran S, Salehi R (2017) Development and characterization of PLA-mPEG copolymer containing iron nanoparticle-coated carbon nanotubes for controlled delivery of Docetaxel. Polymer 117:117–131
12. Meehan C, Banat IM, McMullan G, Nigam P, Smyth F, Marchant R (2000) Decolorization of Remazol Black-B using a thermotolerant yeast, *Kluyveromyces marxianus* IMB3. Environ Int 26(1–2):75–79
13. Otero M, Rozada F, Calvo LF, Garcıa AI, Moran A (2003) Kinetic and equilibrium modelling of the methylene blue removal from solution by adsorbent materials produced from sewage sludges. Biochem Eng J 15(1):59–68
14. Chen KC, Wu JY, Liou DJ, Hwang SCJ (2003) Decolorization of the textile dyes by newly isolated bacterial strains. J Biotechnol 101(1):57–68
15. Alkan M, Demirbaş Ö, Çelikçapa S, Doğan M (2004) Sorption of acid red 57 from aqueous solution onto sepiolite. J Hazard Mater 116(1–2):135–145
16. Ho YS, Chiang TH, Hsueh YM (2005) Removal of basic dye from aqueous solution using tree fern as a biosorbent. Process Biochem 40(1):119–124
17. Bouzaida I, Rammah MB (2002) Adsorption of acid dyes on treated cotton in a continuous system. Mater Sci Eng, C 21(1–2):151–155
18. Walker GM, Hansen L, Hanna JA, Allen SJ (2003) Kinetics of a reactive dye adsorption onto dolomitic sorbents. Water Res 37(9):2081–2089
19. Wong YC, Szeto YS, Cheung W, McKay G (2004) Adsorption of acid dyes on chitosan—equilibrium isotherm analyses. Process Biochem 39(6):695–704
20. Mall ID, Srivastava VC, Agarwal NK, Mishra IM (2005) Removal of congo red from aqueous solution by bagasse fly ash and activated carbon: kinetic study and equilibrium isotherm analyses. Chemosphere 61(4):492–501
21. Robinson T, Chandran B, Nigam P (2002) Removal of dyes from a synthetic textile dye effluent by biosorption on apple pomace and wheat straw. Water Res 36(11):2824–2830
22. Foroutan R, Peighambardoust SJ, Boffito DC, Ramavandi B (2022) Sono-photocatalytic activity of cloisite 30B/ZnO/Ag2O

nanocomposite for the simultaneous degradation of crystal violet and methylene blue dyes in aqueous media. Nanomaterials 12(18):3103
23. Ho YS, Chiu WT, Wang CC (2005) Regression analysis for the sorption isotherms of basic dyes on sugarcane dust. Biores Technol 96(11):1285–1291
24. Özer A, Akkaya G, Turabik M (2006) Biosorption of acid blue 290 (AB 290) and acid blue 324 (AB 324) dyes on Spirogyra rhizopus. J Hazard Mater 135(1–3):355–364
25. Crini G (2005) Biores. Technol. In press
26. Dönmez G, Aksu Z (2002) Removal of chromium (VI) from saline wastewaters by Dunaliella species. Process Biochem 38(5):751–762
27. Tien CJ (2002) Biosorption of metal ions by freshwater algae with different surface characteristics. Process Biochem 38(4):605–613
28. Shukla A, Zhang YH, Dubey P, Margrave JL, Shukla SS (2002) The role of sawdust in the removal of unwanted materials from water. J Hazard Mater 95(1–2):137–152
29. Khatooni H, Peighambardoust SJ, Foroutan R, Mohammadi R, Ramavandi B (2023) Adsorption of methylene blue using sodium carboxymethyl cellulose-g-poly (acrylamide-co-methacrylic acid)/Cloisite 30B nanocomposite hydrogel. J Polym Environ 31(1):297–311
30. Özer A, Akkaya G, Turabik M (2006) The removal of Acid Red 274 from wastewater: combined biosorption and biocoagulation with Spirogyra rhizopus. Dyes Pigm 71(2):83–89
31. Çetinkaya HF, Cebeci MS, Kaya S, Jalbani NS, Maslov MM, Marzouki R (2023) Removal of erythrosine B dye from wastewater using chitosan boric acid composite material: Experimental and density functional theory findings. J Phys Org Chem 36(12):e4400
32. Çelik MS, Çetinus ŞA, Yenidünya AF, Çetinkaya S, Tüzün B (2023) Biosorption of Rhodamine B dye from aqueous solution by Rhus coriaria L. plant: equilibrium, kinetic, thermodynamic and DFT calculations. J Mol Struct 1272:134158
33. Celik MS, Kütük N, Yenidünya AF, Çetinkaya S, Tüzün B (2023) Removal of safranin O from wastewater using Streptomyces griseobrunneus dead biomass and in silico calculations. Biomass Convers Bior 1–12
34. Perdew JP, Burke K, Ernzerhof M (1996) Generalized gradient approximation made simple. Phys Rev Lett 77(18):3865
35. Francl MM, Pietro WJ, Hehre WJ, Binkley JS, Gordon MS, DeFrees DJ, Pople JA (1982) Self-consistent molecular orbital methods. XXIII. A polarization-type basis set for second-row elements. J Chem Phys 77(7):3654–3665
36. Ufimtsev IS, Martínez TJ (2009) Quantum chemistry on graphical processing units. 3. Analytical energy gradients and first principles molecular dynamics. J Chem Theo Comp 5:2619
37. Titov AV, Ufimtsev IS, Luehr N, Martinez TJ (2013) Generating efficient quantum chemistry codes for novel architectures. J Chem Theory Comput 9(1):213–221
38. Wang LP, Song C (2016) Geometry optimization made simple with translation and rotation coordinates. J Chem Phys 144(21)
39. Grimme S, Antony J, Ehrlich S, Krieg H (2010) A consistent and accurate *ab initio* parametrization of density functional dispersion correction (DFT-D) for the 94 elements H-Pu. J Chem Phys 132:154104
40. Çelik MS, Çaylak O, Kütük N, Yenidünya AF, Çetinkaya S, Maslov MM, Kaya S (2024) Removal of lead ions (Pb^{2+}) from aqueous solution using chitosan/starch composite material: experimental and density functional theory findings. Biomass Convers Bioref 1–16
41. Çetinkaya S, Kaya S, Aksu A, Çetintaş Hİ, Jalbani NS, Erkan S, Marzouki R (2023) Equilibrium and DFT modeling studies for the biosorption of Safranin O dye from water samples using Bacillus subtilis biosorbent. J Mol Struct 1276:134761
42. Al-Qodah Z, Al-Shannag M, Amro A, Bob M, Bani-Melhem K, Alkasrawi M (2017) Impact of surface modification of green algal biomass by phosphorylation on the removal of copper (II) ions from water. Turk J Chem 41(2):190–208
43. Verma DK, Khan F (2016) Green approach to corrosion inhibition of mild steel in hydrochloric acid medium using extract of spirogyra algae. Green Chem Lett Rev 9(1):52–60
44. Gupta VK, Rastogi A (2008) Biosorption of lead from aqueous solutions by green algae Spirogyra species: kinetics and equilibrium studies. J Hazard Mater 152(1):407–414
45. Moon SA, Salunke BK, Saha P, Deshmukh AR, Kim BS (2018) Comparison of dye degradation potential of biosynthesized copper oxide, manganese dioxide, and silver nanoparticles using Kalopanax pictus plant extract. Korean J Chem Eng 35:702–708
46. Hebert J, Wang L, Wang X, Baker J, Rivera N, Troedel M, Li Z (2021) Mechanisms of Safranin O interaction with 1: 1 layered clay minerals. Sep Sci Technol 56(12):1985–1995
47. Venkata Mohan S, Ramanaiah SV, Rajkumar B, Sarma PN (2007) Removal of fluoride from aqueous phase by biosorption onto algal biosorbent Spirogyra sp.-IO2: sorption mechanism elucidation. J Hazard Mater 141(3):465–74
48. de Araujo CMB, Wernke G, Ghislandi MG, Diório A, Vieira MF, Bergamasco R, Rodrigues AE (2023) Continuous removal of pharmaceutical drug chloroquine and Safranin-O dye from water using agar-graphene oxide hydrogel: Selective adsorption in batch and fixed-bed experiments. Environ Res 216:114425
49. Kamel MM, Alsohaimi IH, Alhumaimess MS, Hassan HM, Alshammari MS, El-Sayed MY (2021) A glassy polyvinyl alcohol/silica gel hybrid composite for Safranin removal: adsorption, kinetic and thermodynamic studies. Res Chem Intermed 47:925–944
50. Sayyaf H, Mostafaii GR, Iranshahi L, Mosavi GA, Aseman E (2016) Removal of Cr (VI) from synthetic aqueous solutions by filamentous green algae Spirogyra porticalis. Desalin Water Treat 57(39):18438–18445
51. Adebowale KO, Olu-Owolabi BI, Chigbundu EC (2014) Removal of Safranin-O from aqueous solution by adsorption onto kaolinite clay. J Encapsul Adsorption Sci 4(03):89
52. Mahmoodi NM (2014) Synthesis of core–shell magnetic adsorbent nanoparticle and selectivity analysis for binary system dye removal. J Ind Eng Chem 20(4):2050–2058
53. Kütük N (2022) Congo red biosorption with dried mint leaves; ısotherm and kinetic studies. European J Sci Technol 42:113–117
54. Danish M, Ahmad T, Majeed S, Ahmad M, Ziyang L, Pin Z, Iqubal SS (2018) Use of banana trunk waste as activated carbon in scavenging methylene blue dye: kinetic, thermodynamic, and isotherm studies. Bioresour Technol Reports 3:127–137
55. Çiçekci A, Dönmez B, Kavcı E, Laçin Ö (2020) Adsorption isotherm and thermodynamics of malachite green on peach seed shell. Sinop Univ J Sci 5(2):103–111
56. Errais E, Duplay J, Darragi F, M'Rabet I, Aubert A, Huber F, Morvan G (2011) Efficient anionic dye adsorption on natural untreated clay: kinetic study and thermodynamic parameters. Desalination. 275(1–3):74–81
57. Salem MA, Salem IA, Zaki HM, El-Sawy AM (2022) Elimination of Safranin-O and a binary mixture of Safranin-O and methylene blue from water by adsorption on magnetite/Ag nanocomposite. Egypt J Pet 31(2):39–49
58. Phuong DTM, Loc NX (2022) Rice straw biochar and magnetic rice straw biochar for Safranin O adsorption from aqueous solution. Water 14(2):186
59. Fakhry H, Hassan HM, El-Aassar MR, Alsohaimi IH, Hussein MF, ALQahtani MM, El-Amier YA, (2022) A treatment of wastewater containing Safranin O using immobilized Myriophyllum spicatum L. onto polyacrylonitrile/polyvinylpyrrodlidone biosorbent. J Inorg Organomet Polym Mater 32(8):3181–3195

60. Mullerova S, Baldikova E, Prochazkova J, Pospiskova K, Safarik I (2019) Magnetically modified macroalgae Cymopolia barbata biomass as an adsorbent for Safranin O removal. Mater Chem Phys 225:174–180
61. Baytar O, Ceyhan AA, Şahin Ö (2018) Investigation of Pb(II) adsorption from aqueous solutions using activated carbon obtained from buckwheat seeds: isotherm and kinetics. Bitlis Eren Univ J Sci 7(2):256–267
62. Li H, Wang F, Li J, Deng S, Zhang S (2021) Adsorption of three pesticides on polyethylene microplastics in aqueous solutions: kinetics, isotherms, thermodynamics, and molecular dynamics simulation. Chemosphere 264:128556
63. Joudi M, Nasserlah H, Hafdi H, Mouldar J, Hatimi B, Muhammedi ME, Bakasse M (2020) Synthesis of an efficient hydroxyapatite–chitosan–montmorillonite thin film for the adsorption of anionic and cationic dyes: adsorption isotherm, kinetic and thermodynamic study. SN Appl Sci 2:1–13
64. Pakdel PM, Peighambardoust SJ, Arsalani N, Aghdasinia H (2022) Safranin-O cationic dye removal from wastewater using carboxymethyl cellulose-grafted-poly (acrylic acid-co-itaconic acid) nanocomposite hydrogel. Environ Res 212:113201

Publisher's Note Springer Nature remains neutral with regard to jurisdictional claims in published maps and institutional affiliations.